RSC Advances

PAPER

View Article Online
View Journal | View Issue

Cite this: *RSC Adv.*, 2024, **14**, 9985

Dual mechanisms in hydrogen reduction of copper oxide: surface reaction and subsurface oxygen atom transfer

Yehan Wu,[a] Ruixue Fang,[a] Laihong Shen *[a] and Hongcun Bai[b]

The study of the reduction of copper oxide (CuO) by hydrogen (H_2) is helpful in elucidating the reduction mechanism of oxygen carriers. In this study, the reduction mechanism of CuO by H_2 and the process of oxygen atom transfer were investigated through the density functional theory (DFT) method and thermodynamic calculation. DFT calculation results showed that during the reaction between H_2 and the surface of CuO, Cu underwent a $Cu^{2+} \rightarrow Cu^{1+} \rightarrow Cu^0$ transformation, the Cu–O bond (−IpCOHP = 2.41) of the Cu_2O phase was more stable than that (−IpCOHP = 1.94) of the CuO phase, and the reduction of Cu_2O by H_2 was more difficult than the reduction of CuO. As the surface oxygen vacancy concentration increased, it was more likely that the subsurface O atoms transfer to the surface at zero H_2 coverage (no H_2 molecule on the surface), allowing the surface to maintain a stable Cu_2O phase. However, when the H_2 coverage was 0.25 monolayer (ML) (one H_2 molecule every four surface Cu atoms), the presence of H atoms on the surface made the upward transfer of O atoms from the subsurface more difficult. The rate of consuming surface O atoms in the reduction reaction was greater than the rate of subsurface O atom transfer induced by the reduction reaction and the surface Cu_2O phase could not be maintained stably. Through thermodynamic analysis, at high H_2 concentration, the reaction between H_2 and CuO was more likely to generate Cu, while at low H_2 concentration, it was more likely to generate Cu_2O. In summary, the valence state of Cu in the reaction process between CuO and H_2 depended on the concentration of H_2.

Received 18th February 2024
Accepted 18th March 2024

DOI: 10.1039/d4ra01240b

rsc.li/rsc-advances

1 Introduction

Chemical looping combustion (CLC) has been shown to be a promising combustion technology for power production with integrated CO_2 capture.[1–3] In CLC, a metal oxide that acts as an oxygen carrier is alternately reduced by a fuel (syngas or natural gas) in a fuel reactor and oxidized by air in an air reactor. CuO is a good oxygen carrier for chemical looping combustion.[4–6] CuO undergoes a reduction process in the fuel reactor. Numerous studies have been carried out on CuO. However, the reduction mechanism of CuO, especially the influence of reducing gas concentration, is currently unclear. Hydrogen (H_2) is the most common reducing gas. There were many studies on the reduction of CuO by H_2. The reaction of H_2 with CuO was experimentally studied using *in situ* X-ray diffraction by Kim *et al.*[7] Samples were loaded in an open sapphire capillary having an inner diameter of 0.5 mm. An inlet gas was a 5% H_2 and 95% He gas mixture. The results showed that under high H_2 flow rate ($\approx$15 cm^3 min^{-1}), CuO can be directly reduced to metallic Cu ($Cu^{2+} \rightarrow Cu^0$). During the reduction process, no evidence of any intermediate state (Cu^+) was found. Cu_2O appeared as an intermediate phase only at very low H_2 flow rates (<1 cm^3 min^{-1}); this result has been supported by multiple studies.[8–11]

Maimaiti *et al.*[12] investigated the process of H_2 reduction on the surface of CuO using the density functional theory (DFT) method and concluded that Cu^+ appeared during the reaction. This could not explain the experimentally observed phenomenon that Cu^{2+} is directly converted into the Cu^0 phase under high H_2 concentration. This may be due to the fact that, in addition to the reaction between H_2 and the CuO surface, other reaction processes are involved in the reduction reaction. Using the DFT method, Jabraoui *et al.*[13] found that oxygen vacancies play an important role in the decomposition of CuO to release O_2. Oxygen vacancies on the surface can promote the transfer of internal O to the surface. Yang *et al.*[14] found that rearrangements occurred on the CuO surface as the concentration of surface oxygen vacancies increased. Transition in the surface structure caused by the reaction between H_2 and CuO may in turn affect the reaction between H_2 and CuO.

In this study, the DFT method was adapted to study the reaction between H_2 and the CuO surface initially. Subsequently, subsurface O atom transfer was studied with different

[a]*Key Laboratory of Energy Thermal Conversion and Control of Ministry of Education, School of Energy and Environment, Southeast University, Nanjing 210096, China*
[b]*State Key Laboratory of High-efficiency Utilization of Coal and Green Chemical Engineering, Ningxia University, Yinchuan, Ningxia 750021, China*

H_2 coverages (0 ML, 0.25 ML) by DFT. DFT provided a precise approach[15,16] to the theoretical problem of electronic structure. Both the climbing image nudged elastic band (CI-NEB)[17] and dimer[18] methods were applied to find the transition states. The transition state structure of chemical reactions could help us better understand the kinetic properties of chemical reactions. Thermodynamic calculations were applied to the reactions occurring in the H_2 reduction of CuO process.

2 Methodology and model

2.1 Computational methodology

All DFT calculations were performed using the software Vienna *ab initio* simulation package (VASP).[19,20] The projector augmented wave (PAW) method was chosen for the calculations to handle the effect of the core electrons on the valence electrons.[21] The Perdew–Burke–Ernzerhof (PBE) exchange function under the generalized gradient approximation (GGA) was selected.[22] The Monkhorst–Pack method was used to sample the Brillouin zone,[23] and *k*-point grids with sizes of $8 \times 8 \times 8$ and $4 \times 4 \times 1$ were used for CuO unit cells and CuO slab calculations, respectively. The plane wave cutoff energy was 400 eV. Because the conventional DFT functionals cannot accurately describe the strong correlation effect between the Cu 3d orbital electrons in CuO,[24] the GGA+*U* method[25] was used in order to accurately describe the strongly correlated, highly localized 3d electrons in CuO. To describe the Cu atom, $U = 7$ eV and $J = 0.98$ eV were used.[26] The electron energy was relaxed to an accuracy of 10^{-6} eV, and the atomic positions were optimized until the Hellmann–Feynman force was less than 0.02 eV $Å^{-1}$. Projected crystal orbital Hamilton population (pCOHP) calculations were conducted using the LOBSTER code.[27] The structures were visualized by VESTA software.[28] Thermodynamic calculations were conducted using the HSC Chemistry 6.0 software. For H_2 adsorption on the CuO surface, the energy of gas adsorption is

$$E_{ads} = E(H_2\text{-surface}) - E(\text{surface}) - E(H_2) \quad (1)$$

where E_{ads} is the gas adsorption energy, $E(H_2\text{-surface})$ is the total energy of the system after H_2 is adsorbed to the CuO surface, $E(\text{surface})$ is the total energy of the CuO surface, and $E(H_2)$ is the total energy of H_2. The activation energy of the reaction is expressed as

$$E_a = E_{TS} - E_{IS} \quad (2)$$

where E_{TS} is the energy of the transition state and E_{IS} is the energy of the initial state. The heat of reaction is

$$\Delta E = E_{FS} - E_{IS} \quad (3)$$

where E_{FS} is energy of the final state. Microscopically, gas concentration can be reflected by the adsorption surface gas coverage (θ).[29] The formula for adsorption gas coverage is as follows:

$$\theta = N_g/N_M \quad (4)$$

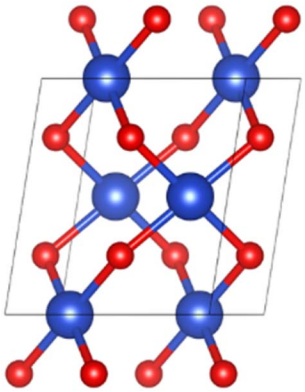

Fig. 1 Unit cell structure of CuO.

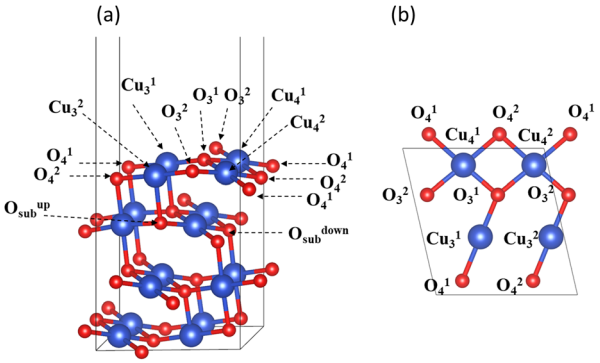

Fig. 2 CuO (111) surface unit cell: (a) front view (b) top view.

where N_g is the number of adsorbed gas molecules, and N_M is the number of surface metal atoms. The unit for θ is monolayer (ML).

2.2 Structural properties

The spatial structure of CuO crystal belonged to the *C*2/*c* group.[30] Fig. 1 illustrates the unit cell structure of CuO. The CuO unit cell parameters were calculated as $a = 4.63$ Å, $b = 3.43$ Å, $c = 5.09$ Å, $\beta = 99.43°$, and the Cu–O bond length was 1.95 Å, which was well aligned with experimental data,[30] proving that the chosen parameter settings were appropriate.

Experiments and calculations have both demonstrated that CuO (111) is the most stable surface of copper oxide and the surface most easily observed in experiments.[31,32] Therefore, the CuO surface model used in this study was CuO (111), as shown in Fig. 2. The CuO (111) surface used for hydrogen reduction and surface structure calculation was a (2×1) supercell that retains four layers of atoms. The thickness of the vacuum layer was 15 Å. The lower two of these layers were fixed, and the upper two were relaxed. Inside the unit cell, there were a total of four oxygen atoms on the surface of CuO (111), which were divided into two categories according to the coordination number. The oxygen atoms with a coordination number of three were labeled O_3^1 and O_3^2, and those with a coordination number of four were labeled O_4^1 and O_4^2. There were four Cu atoms on the surface in total, namely, the three-coordinated Cu_3^1 and Cu_3^2 and the four-coordinated Cu_4^1 and Cu_4^2.

3 Results and discussion

3.1 Study of the complete reaction paths of hydrogen on copper oxide surface

On the surface of intact copper oxide, two H_2 adsorption sites were considered: the top sites of the three-coordinated Cu and four-coordinated Cu atoms. On the intact CuO surface, the adsorption energy E_{ads} of H_2 on Cu_3^1 was −2.30 kJ mol^{-1}, and E_{ads} of H_2 on Cu_4^1 was −2.01 kJ mol^{-1}. H_2 adsorption on the intact surface of CuO released very little heat, indicating that no chemisorption occurred. However, H_2 adsorption on the three-coordinated Cu_3^1 still released more energy, and it could be assumed that H_2 was initially adsorbed on the three-coordinated Cu_3^1.

Next, the type of O that H_2 reacts with first on the surface was considered. The reaction heat ΔE between H_2 and O_3^1 was −182.50 kJ mol^{-1} and that between H_2 and O_4^1 was −93.31 kJ mol^{-1}.

H_2 was more likely to combine with the three-coordinated O atoms on the surface of CuO to form H_2O, so H_2 would react with the three-coordinated O on the surface of CuO first, and then with the four-coordinated O afterward. This has also been confirmed by calculations by Maimaiti *et al.*[12]

The reaction of H_2 with the CuO surface is divided into two parts. First, the dissociation of H_2, and then the formation of H_2O from the two dissociated H atoms and a surface O atom. H_2 dissociates in two ways on the surface of metal oxides:[33–36] the first is the dissociation of H_2 to form H^- and H^+, which are adsorbed on the metal and oxygen sites, respectively, producing M–H and O–H groups (path 1); the other is the dissociation of H_2 to produce two H atoms, which combine with two O atoms to form two O–H groups (path 2). Both H_2 dissociation pathways are possible during the H_2 reduction of CuO. The two reaction paths of H_2 with CuO are shown in Fig. 3. The energy changes in the process for the two different reactions paths are shown in Fig. 4. In path 1, from 1A to FS was the rate-determining step. In path 2, from 1A′ to FS was the rate-determining step. In path 2, the rate-determining step was an endothermic reaction, which increased the difficulty of the reaction. X_a was used to measure the similarity between the initial and final states, *i.e.*, the root sum squared of the distance between the initial and final states of the corresponding atoms. The smaller X_a was, the smaller the distance of the atom movement before and after the reaction was. In path 1, the X_a between 1A and IS was 2.45, and the X_a between FS and 1A was 3.68. In path 2, the X_a between 1A′ and IS was 3.89, and the X_a between FS and 1A′ was 4.09. From the perspective of H atom diffusion, in path 2, H atoms required more diffusion movement, which increased the difficulty of the reaction in path 2. Hence, the H_2 dissociation approach chosen in this study is path 1.

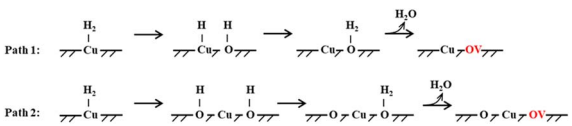

Fig. 3 Two H_2 dissociation modes and CuO reaction paths.

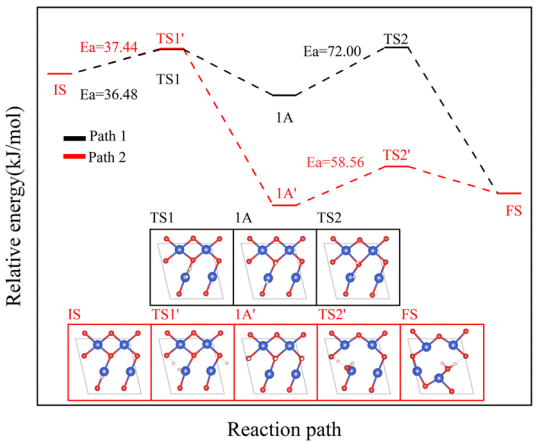

Fig. 4 The two reaction paths of H_2 with CuO (the white atom is the H atom).

Next, the full-path process of H_2 reduction in the surface reaction of CuO was studied by DFT method.

In the process of complete reduction of CuO by H_2, as the reaction of H_2 with surface O atoms proceeds, H_2O is formed on the surface of CuO (111) with different oxygen vacancy concentrations until no O atoms remain on the surface. As shown in Fig. 5, for convenience, this article refers to the surfaces of CuO (111) with 25%, 50%, 75%, and 100% oxygen vacancy concentration as surface I, surface II, surface III, and surface IV, respectively. This designation was used to study the effect of different oxygen vacancy concentrations on the reaction between CuO and H_2. The complete reaction process of H_2 with the CuO (111) surface is shown in Fig. 6.

On the intact surface, the initial state was a state when H_2 adsorbed on the top site of Cu_3^1, and the H–H bond length of the adsorbed H_2 molecule was 0.75 Å, which was essentially unchanged compared to the H–H bond length of the gaseous H_2 molecules (0.74 Å). Then, the H–H bond in the H_2 molecule was broken to form an H–O group, and another H atom stayed in the top site of the Cu atom. During this process, the Cu–O bonds were activated, and the Cu–O bonds around O_3^1 lengthened. Subsequently, another H atom was combined with O_3^1 to form two H–O bonds on the surface. The two H–O bonds' lengths were 0.97 Å and 1.03 Å, respectively, and the H–O–H bond angle was 106.40°. In the H_2O molecule, the H–O bond length is 0.99 Å, and the H–O–H bond angle is 104.5°. It can be considered that water molecules were generated on the surface.

On surface I, when H_2 was adsorbed on the top site of Cu_3^1, the H–H bond length was 0.80 Å, and the H–H bond was activated. The Cu–O bond around O_3^2 was longer than that of the intact CuO surface, and when an H–O bond was formed, the Cu–O bonds were also more active than the ones on intact surfaces. Compared to the intact surface, on surface I, the energy barrier for the reaction between H_2 and O_3^2 atoms to form H_2O molecules was smaller, the reaction was more likely to occur, and more heat was given off by the entire reaction process. During the reaction, the O atoms on the surface were rearranged, with O_4^1 on the surface migrating to the original

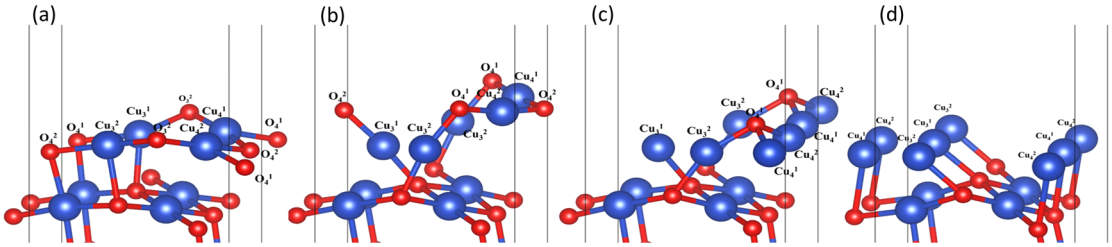

Fig. 5 Surfaces with different oxygen vacancy concentrations as the reaction of H_2 reduction of CuO occurs: (a) surface I (25% oxygen vacancy concentration), (b) surface II (50% oxygen vacancy concentration), (c) surface III (75% oxygen vacancy concentration), and (d) surface IV (100% oxygen vacancy concentration).

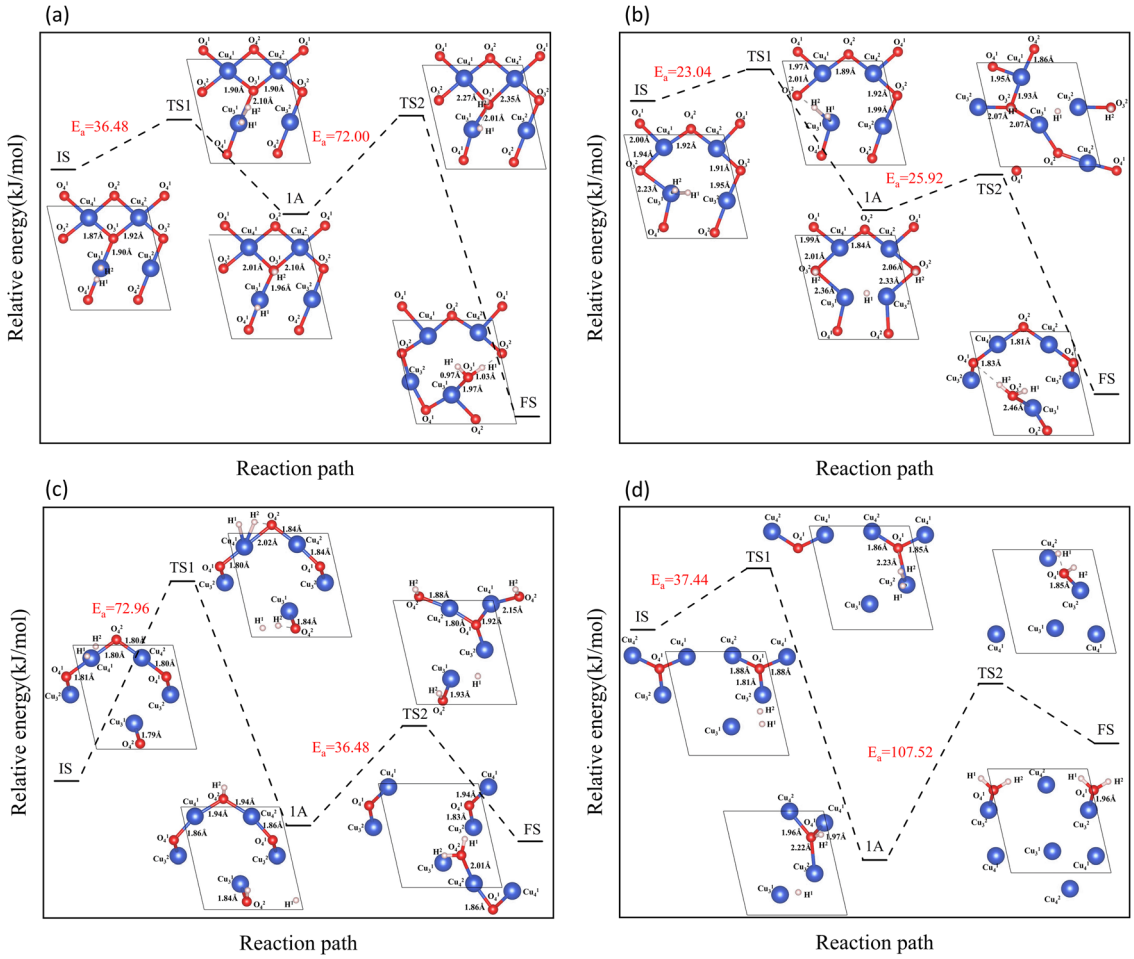

Fig. 6 Entire process of the reaction path of H_2 reduction on the CuO surface: (a) H_2 reacts with an intact surface, (b) H_2 reacts with surface I, (c) H_2 reacts with surface II, (d) H_2 reacts with surface III.

position of O_3^2. With the dissociation of H_2O, a CuO surface with a 50% oxygen vacancy concentration, which has been denoted as surface II, was formed.

On surface II, the arrangement of Cu and O was similar to the (111) surface of Cu_2O.[37] The length of the Cu–O bond on this surface was shorter than that on both previous surfaces. At the initial state, H_2 adsorbed on the top site of Cu, and the H–H bond length of the H_2 molecule was 0.75 Å. They were not activated. The process of cleavage of H_2 molecules and formation of an H–O bond had a higher energy barrier. The required energy to break the barrier for the subsequent formation of two H–O bonds was reduced but still high compared to the same reaction process on surface I.

On surface III, H_2 cannot adsorb on the top sites of Cu, but instead adsorbed on the hollow sites on Cu atoms. The H–H bond length of the adsorbed H_2 molecule was 0.75 Å. During the cleavage of the H_2 molecule and the formation of an H–O bond, the required energy barrier was similar to the energy required

Table 1 Bader charge values of surface atoms under different oxygen vacancy concentration conditions and Cu atoms in CuO, Cu_2O, and Cu bulks

Bader charge/*e*										
	Atom									
Surface	Cu_3^1	Cu_3^2	Cu_4^1	Cu_4^2	O_3^1	O_3^2	O_4^1	O_4^2	Bulk	Cu
Intact surface	10.24	10.24	10.02	10.02	6.90	6.90	6.91	6.91	CuO	10.00
Surface I	10.37	10.36	10.27	10.28		6.99	6.90	6.95		
Surface II	10.44	10.46	10.41	10.41			6.93	6.95	Cu_2O	10.46
Surface III	10.73	10.50	10.71	10.67			6.92			
Surface IV	10.77	10.77	10.86	10.86					Cu	10.99

for the first step of the reaction on the intact surface. The higher energy required in the formation of two H–O bonds may be due to the fact that more energy was required to rearrange the surface Cu atoms as more surface oxygen vacancies appeared.

In summary, the complete reduction of the CuO surface by H_2 was calculated. The first chemical process in the two-step reaction was mainly the cleavage of the H_2 molecule, the activation of the Cu–O bond, and the formation of the H–O bond. The second step was mainly the breaking of the Cu–O bond and the formation of the H–O–H bond. As the concentration of oxygen vacancies on the surface increased, the reaction between H_2 and CuO was more intense on the surface with a 25% oxygen vacancy concentration. The reaction between H_2 and CuO became more difficult and slowed down as the concentration of oxygen vacancies continued to increase.

3.2 Electronic structure analysis

Table 1 lists the Bader charge on the intact surface and on surfaces with four different oxygen vacancy concentrations (0%, 25%, 75%, and 100%), as well as the Bader charge of Cu atoms in CuO, Cu_2O, and Cu bulks. According to the Bader charge results, it is concluded that on the intact surface, the three-coordinated Cu atoms carry more charge than the four-coordinated Cu atoms, which confirms the choice of three-coordinated Cu as the initial adsorption site for H_2. The Bader charge of the O atom remained stable throughout the reaction. This was because the O atom is more electronegative with respect to the Cu atom and therefore always attracts charge to fill its empty orbitals. The Bader charge of the Cu atom increased as the reaction proceeded. Compared with the Bader charge of Cu atom in CuO bulk, on the intact surface, the four-coordinated Cu atoms were at +2 valence, and the three-coordinated Cu atoms were at +2 valence approximately because of the presence of surface dangling bonds. On surface II, the Bader charge of the Cu atoms were near the Bader charge of Cu atom in Cu_2O bulk. Each Cu atom had two coordination bonds, which was consistent with the Cu atom in Cu_2O bulk. It could be considered that the valence state of Cu atoms on surface II was +1. On surface IV, Cu atoms had no coordination bonds on the surface and only had one coordination bond with the O atoms on the subsurface. Comparing the Bader charge of Cu atoms on surface IV with the Bader charge of Cu atom in Cu bulk, it could be approximated that the Cu atoms on surface IV were at 0 valence. Therefore, during the reduction of a CuO surface by H_2, the Cu atoms on the entire surface exhibited a change process of $Cu^{2+} \rightarrow Cu^{1+} \rightarrow Cu^0$. Based on the calculation of the transition state, it was found that it is more difficult to reduce Cu^{1+} than Cu^{2+}, a result that has also been confirmed by experiments.[9]

The molecular orbitals before H_2 adsorption consisted of the σ_{1s} bonding orbital formed by the 1s orbitals of the two H atoms, and the σ_{1s}^* antibonding orbital.[38] The σ_{1s}^* antibonding orbitals were mainly located above the Fermi energy level, and with a small projected density of states (PDOS), so the electrons of H_2 were mainly concentrated in the σ_{1s} bonding orbitals. The valence charge of the Cu atom was concentrated in the 3d orbital, which was the active orbital of the Cu atom.[39] Fig. 7 shows the PDOS plots of H 1s and Cu 3d before and after H_2 adsorption on different surfaces. On the intact CuO surface, after H_2 adsorption, the 1s orbitals of H were transferred to a lower energy level, whereas the 3d orbitals of Cu remain almost unchanged. The small overlap region between the two suggests that the hybridization between the 1s orbital of H and 3d orbital of Cu is weak, which corresponds to the relatively low adsorption energy. On surface I, the 1s orbitals of H and 3d orbitals of Cu after H adsorption generated new PDOS peaks at lower energy levels and overlapped. This indicated that, when H_2 was adsorbed on surface I, hybrid bonding occurred between the 1s orbital of the H atom and the 3d orbital of Cu, forming a bonding orbital with lower energy, which increased the adsorption energy. At the same time, the original σ_{1s} and σ_{1s}^* molecular orbitals of H_2 were destroyed, which led to the activation of the covalent bond of H_2, which was conducive to the subsequent dissociation and diffusion of the H_2. On surfaces II and III, after H adsorption, the H 1s orbital of moved to a lower energy level, the 3d orbital of Cu remained essentially unchanged, and the region of overlap between the two was relatively small. This indicated that on both surfaces the reaction with Cu remains weak when H_2 molecular adsorption occurs. The analysis of the PDOS plots led to the conclusion that only surface I activated the covalent bond of H_2 well upon adsorption of H_2, which facilitated the subsequent dissociation of H_2.

To understand the bonding of Cu–O on different surfaces, Fig. 8 illustrates the minus projected crystal orbital Hamilton population (−pCOHP) diagrams of Cu–O bonds on CuO

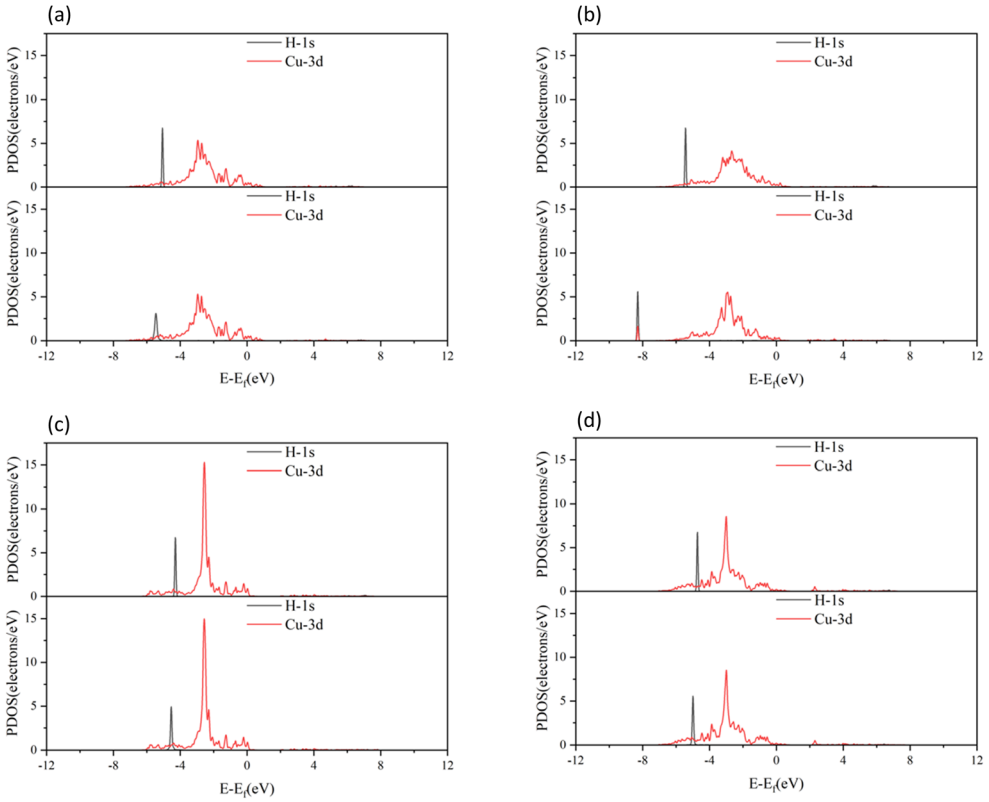

Fig. 7 PDOS plots of H_2 before and after adsorption on different CuO surfaces: (a) H_2 adsorbed on the intact surface, (b) H_2 adsorbed on surface I, (c) H_2 adsorbed on surface II, and (d) H_2 adsorbed on surface III. In all parts, the top figure shows before adsorption, and bottom figure shows after adsorption.

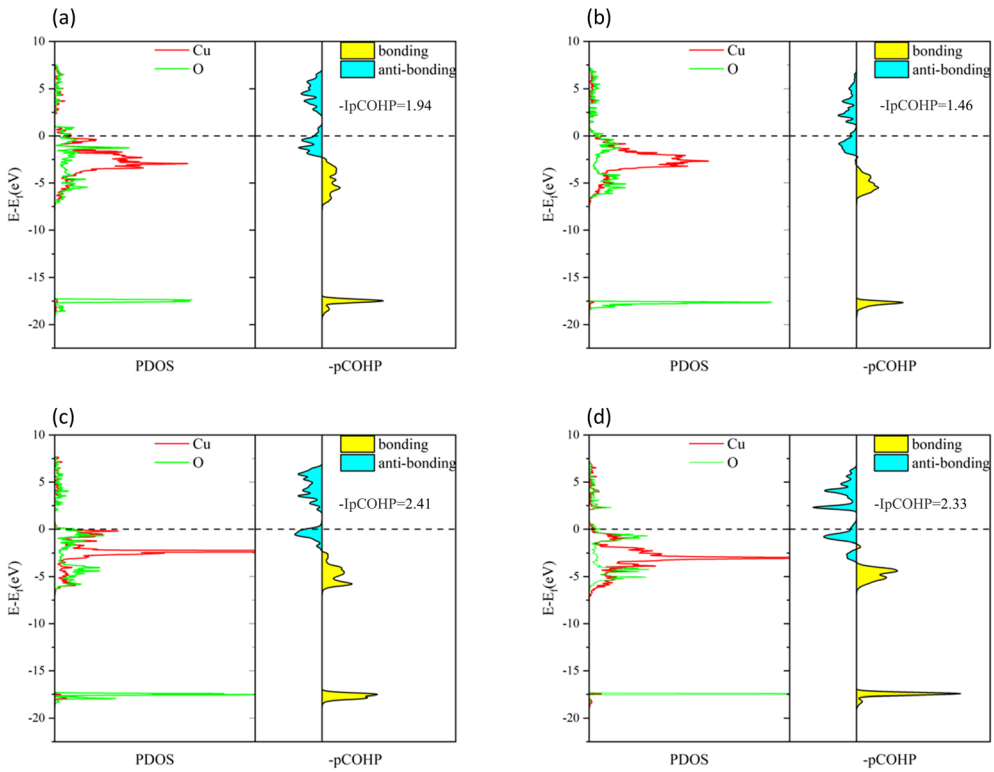

Fig. 8 −pCOHP diagrams of Cu–O bonds on different CuO surfaces: (a) intact surface, (b) surface I, (c) surface II, and (d) surface III.

surfaces with different oxygen vacancy concentrations. The minus integrated projected crystal orbital Hamilton population (−IpCOHP) of the Cu–O bond is showed in Fig. 9. It can be found that the strength of the Cu–O bond decreased as the concentration of oxygen vacancies on the surface increased. However, as the oxygen vacancy concentration continued to increase, the surface structure underwent rearrangement to form the Cu_2O phase. At this point, the strength of Cu–O bond increased again, and then decreased again with further increase in oxygen vacancy concentration. The strength of the Cu–O bond on surface I was reduced, which makes the reaction between H_2 and the CuO surface more likely to occur. Less energy was needed to activate the Cu–O bond, and the entire reaction process occurred more easily. However, with the rearrangement of the surface structure, the strength of the Cu–O bond increased, making the reaction of H_2 with surfaces II and III more difficult again, because the energy requirement for activating the Cu–O bond became higher.

Based on the analysis of the electronic structure, it can be concluded that an appropriate concentration of surface oxygen vacancies enhances the activation capacity of the CuO surface for H_2 molecules and also reduces the strength of the Cu–O bond, which promotes the reaction of H_2 with the surface O atoms. However, an excessive concentration of oxygen vacancies would cause rearrangements on the CuO surface, and the Cu_2O phase formed would reduce the activation capacity for H_2 molecules and enhance the strength of the Cu–O bond. At the same time, during the reduction of CuO by H_2, excess oxygen vacancies caused a drastic rearrangement of Cu atoms on the surface of CuO, which increased the reaction energy barrier.

3.3 Subsurface oxygen transfer

The process of CuO reduction by H_2 is not a single process in which H_2 reacts with surface O atoms, but also involves the movement of subsurface O atoms to the surface. When oxygen vacancies appear on the surface, subsurface O atoms move upward. H_2 reduction of the CuO surface consumes surface O atoms, and the upward movement of O from the subsurface replenishes the surface O atoms. The two processes compete with each other.

The CuO (111) model utilized in this study with zero H_2 coverage is capable of simulating the transfer of subsurface O atoms under very low H_2 concentration. As shown in Fig. 2, in the CuO (111) model, there are a total of two types of subsurface O atoms: one is the upward-connected, four-coordinated O_{sub}^{up} and the other is the downward-connected, four-coordinated O_{sub}^{down}.

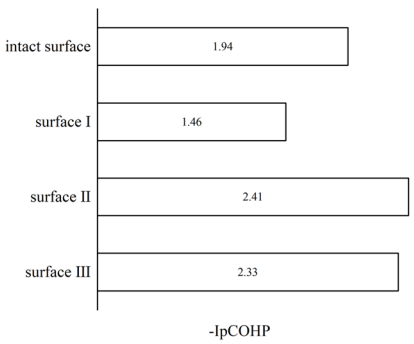

Fig. 9 −IpCOHP diagrams of Cu−O bonds on different CuO surfaces.

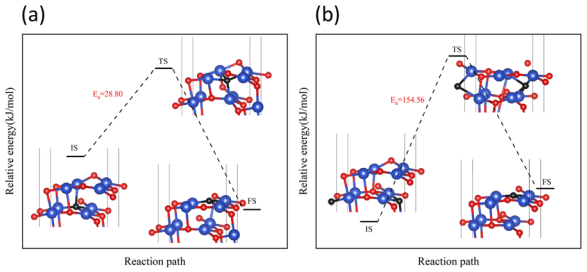

Fig. 10 Transfer paths of two O atoms from the subsurface to the surface: (a) O_{sub}^{up} transfers (b) O_{sub}^{down} transfers.

On surface I, both subsurface O atoms could be transferred to the surface to replenish the O, returning the surface to an intact surface. The energy barriers for the upward transfer of these two O atoms were calculated separately. As shown in Fig. 10, on surface I, for the subsurface O atoms to move to the surface, they must first break the Cu–O bonds formed with the subsurface Cu atoms, reaching the transition state in the process. Subsequently, the O atom was bonded with the Cu atoms of the surface. The energy barrier for upward transfer of O_{sub}^{up} was lower than that of O_{sub}^{down}, and the transfer of O_{sub}^{up} to the surface was easier. However, the energy barrier for upward transfer of O atoms in both cases was higher than that for the reaction of H_2 with O atoms on surface I (Fig. 6(b)). Therefore, for surface I, the rate of upward O replenishment at the subsurface was lower than the rate of surface O consumption by H_2, and the CuO surface became surface II.

Next, the focus was the upward transfer of the subsurface O_{sub}^{up}, as shown in Fig. 11. For surface II, O_{sub}^{up} transferred upward, returning the surface to surface I. The energy barrier is as shown in Fig. 11(a). It can be seen that the energy barrier is very high, and it is difficult for subsurface O to transfer upward. Therefore, the CuO surface changed from surface II to surface III.

However, for surface III, the upward transfer of subsurface O became quite easy, and had the upper hand in the competition with H_2 consumption of O on the surface. The CuO surface returned to surface II; that is, the Cu_2O phase on the surface

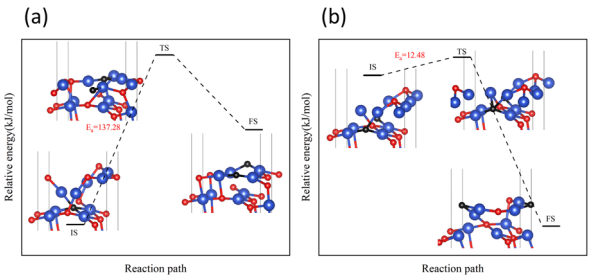

Fig. 11 Transfer path of subsurface O_{sub}^{up} to the surface on (a) surface II, and (b) surface III.

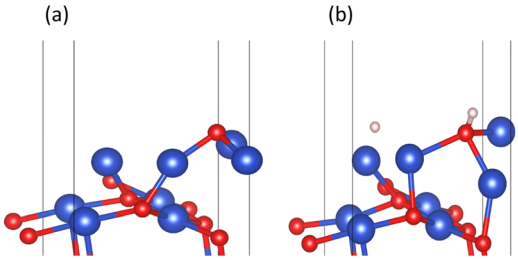

Fig. 12 (a) Surface III and (b) surface III with 0.25 ML H_2 coverage.

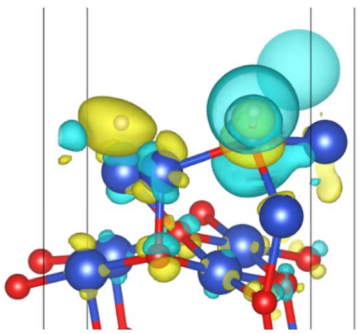

Fig. 13 Surface charge transfer at 0.25 ML H_2 coverage (yellow represents charge increase and blue represents charge decrease).

would remain for a period of time. H_2 continuously consumed O atoms on the surface, and subsurface O atoms were continuously transferred to the surface to replenish it, reaching a dynamic equilibrium. This coincides with the experimental observation of the reaction process $Cu^{2+} \rightarrow Cu^{1+} \rightarrow Cu^0$ under low H_2 concentration.

However, in experiments, the Cu_2O phase[7] was not observed when the H_2 concentration was high. The surface III with H_2 coverage of 0.25 ML could simulate subsurface O atoms transfer under high H_2 concentration, as shown in Fig. 12. This could be considered as having one H_2 molecule on the surface III. However, this H_2 molecule, after dissociation, occupied a surface oxygen vacancy and the top position of an O atom, respectively. Fig. 13 shows the charge transfer on the surface when there are H atoms on the surface. It can be seen that

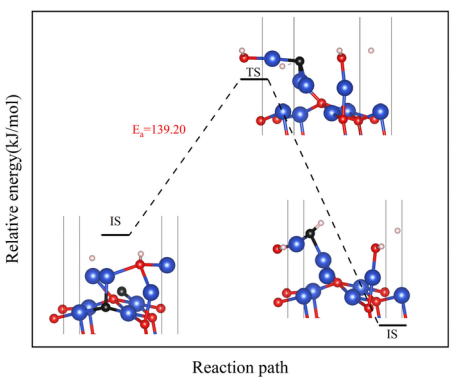

Fig. 14 Transfer path of subsurface O_{sub}^{up} to the surface at 0.25 ML H_2 coverage.

a large amount of charge was distributed around the H atoms on the oxygen vacancies. Fig. 14 illustrates the energy barrier for the O atom transfer process. For surface III, when oxygen vacancies were occupied by H atoms, the upward transfer of oxygen atoms required a large amount of energy to overcome the barrier. The transition state structure no longer occurred in the process of O atoms breaking the Cu–O bond with subsurface Cu atoms. Instead, it occurred in the process of forming H–O bonds between surface O and H. The transfer of subsurface O atoms was particularly difficult when the oxygen vacancies were occupied by H atoms. This may be due to the fact that H–O bonding replaces the original Cu–O bond breaking as a key step in the upward transfer of subsurface O. In the case of a high H_2 concentration, surface III cannot return to surface II, which requires the replenishment of subsurface O. Instead, the surface changes to surface IV due to the reaction of the surface with H_2. Therefore, when the H_2 concentration is high, the Cu_2O phase cannot be stabilized, and only the $Cu^{2+} \rightarrow Cu^0$ process can be observed in the experiment.

3.4 Thermodynamic analysis

The thermodynamic analysis of the H_2 reduction process of CuO was investigated. According to relevant papers on thermodynamics, the change of Gibbs free energy (ΔG) can predict the direction and spontaneity of chemical reactions.[40] Fe_3O_4, Co_3O_4 and NiO are other common oxygen carriers for chemical looping combustion.[41–43] The thermodynamic analysis of the reaction between these other common oxygen carriers and H_2 was used for comparison with the reaction between CuO and H_2. The reactions occurring during the H_2 reduction of CuO and the reactions of other common oxygen carriers with H_2 are listed below.

$$H_2 + 2CuO \rightarrow H_2O + Cu_2O \quad (5)$$

$$H_2 + Cu_2O \rightarrow H_2O + 2Cu \quad (6)$$

$$H_2 + CuO \rightarrow H_2O + Cu \quad (7)$$

$$H_2 + 0.25Fe_3O_4 \rightarrow H_2O + 0.75Fe \quad (8)$$

$$H_2 + 0.25Co_3O_4 \rightarrow H_2O + 0.75Co \quad (9)$$

$$H_2 + NiO \rightarrow H_2O + Ni \quad (10)$$

ΔH and ΔG of each reaction are shown in Fig. 15. All reactions (reaction (5)–(10)) show the same trend. As the temperature increased, both ΔH and ΔG decreased, indicating that the reactions were more favorable at higher temperatures. The reduction of CuO to Cu_2O by H_2 (reaction (5)) released more heat compared to the reduction of Cu_2O to Cu by H_2 (reaction (6)). According to the ΔG, it could be concluded that reducing CuO to Cu_2O by H_2 is easier than reducing Cu_2O to Cu by H_2. The DFT calculation in this study obtained the same result that the reduction of CuO to Cu_2O by H_2 was more likely to occur and released more heat as thermodynamic analysis. The reaction between Fe_2O_3 and H_2 was an endothermic reaction (reaction

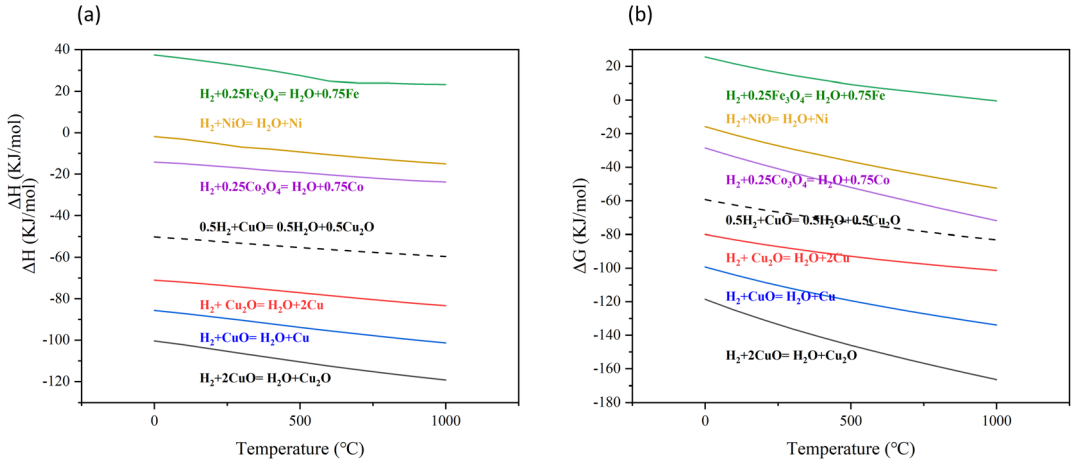

Fig. 15 The trend of Δ*H* and Δ*G* for each reaction with temperature changes.

(8)). The reaction between NiO and H_2 was exothermic, but the heat released was small (reaction (10)). Compared to the reaction between NiO and H_2, the reaction between Co_3O_4 and H_2 released more heat (reaction (9)). However, in contrast to these common oxygen carriers, the reaction between CuO and H_2 released much more heat. The molar ratio of H_2 to CuO in reaction (5) was 1 : 2 and 1 : 1 in reaction (6). Compared to reaction (6), reaction (5) required more CuO at the same molar amount of H_2. It can be observed that when the H_2 concentration was low, the amount of CuO was sufficient, and reaction (5) was thermodynamically favorable. However, as the H_2 concentration increased, the amount of CuO limited the reaction. Under the same amount of CuO, reaction (6) was more likely to occur.

4 Conclusions

In this study, DFT and thermodynamic calculation were used to study the whole process of the reaction between the CuO (111) surface and H_2 as well as the transfer of subsurface O atoms at different H_2 coverage (0 ML, 0.25 ML). Throughout the entire process of H_2 reduction of the CuO (111) surface, the surface Cu atoms underwent the transformation process of $Cu^{2+} \rightarrow Cu^{1+} \rightarrow Cu^0$. As the reaction proceeded, the concentration of surface oxygen vacancies increased, and the CuO surface underwent rearrangement of O atoms to form the Cu_2O phase. The Cu–O bond of the Cu_2O phase was more stable than the Cu–O bond of the CuO phase, and it was therefore more difficult to reduce Cu_2O with H_2 than to reduce CuO. The surface H_2 coverage could reflect the concentration of H_2. As the surface oxygen vacancy concentration increased, it was more likely that the subsurface O atoms transfer to the surface at zero H_2 coverage, allowing the surface to maintain a stable Cu_2O phase. However, when the H_2 coverage was 0.25 ML, the H atoms on the surface hindered the upward transfer of O atoms from the subsurface; therefore, O atoms on the surface was not replenished timely, and the Cu_2O phase could not be maintained stably. Through thermodynamic analysis, compared to other oxygen carriers (Co_3O_4, NiO), the reaction between CuO and H_2 released more heat. The concentration of H_2 affects the reaction products of H_2 with CuO. In summary, the concentration of H_2 affected the valence state of surface Cu by affecting the transfer of subsurface O atoms. It could be considered that as long as the surface oxygen vacancies were occupied by H atoms, subsurface O atoms could not transfer upward in a timely manner, preventing the stable existence of the Cu_2O phase. However, there are various arrangements of H atoms on the surface of CuO, and this study only investigated one particular configuration to examine its impact on subsurface O atom transfer. The study of the effects of different arrangements of H atoms on the surface of CuO will be a primary focus for future research. Meanwhile, AIMD and KMC are two other excellent methods for studying chemical reactions. The application of AIMD and KMC methods will also become the focus of our future work.

Author contributions

Y. Wu performed the calculations and the data analysis and R. Fang prepared the draft of the manuscript. L. Shen initialized the project and proposed the supervision. H. Bai provided the VASP software copyright. All authors have given approval to the final version of the manuscript.

Conflicts of interest

There are no conflicts to declare.

Acknowledgements

This work was supported by the National Natural Science Foundation of China (grants no. 52376099).

References

1 J. Adánez, P. Gayán, I. Adánez-Rubio, *et al.*, Use of chemical-looping processes for coal combustion with CO_2 capture, *Energy Procedia*, 2013, **37**, 540–549.

2 E. M. Eyring, G. Konya, J. S. Lighty, *et al.*, Chemical looping with copper oxide as carrier and coal as fuel, *Oil Gas Sci. Technol.*, 2011, **66**(2), 209–221.
3 M. M. Hossain and H. I. de Lasa, Chemical-looping combustion (CLC) for inherent CO_2 separations—a review, *Chem. Eng. Sci.*, 2008, **63**(18), 4433–4451.
4 S. Jiang, L. Shen, J. Wu, *et al.*, The investigations of hematite-CuO oxygen carrier in chemical looping combustion, *Chem. Eng. J.*, 2017, **317**, 132–142.
5 I. Adánez-Rubio, P. Gayán, F. García-Labiano, *et al.*, Development of CuO-based oxygen-carrier materials suitable for Chemical-Looping with Oxygen Uncoupling (CLOU) process, *Energy Procedia*, 2011, **4**, 417–424.
6 C. R. Forero, P. Gayán, F. García-Labiano, *et al.*, High temperature behaviour of a CuO/γAl_2O_3 oxygen carrier for chemical-looping combustion, *Int. J. Greenhouse Gas Control*, 2011, **5**(4), 659–667.
7 J. Y. Kim, J. C. Hanson, A. I. Frenkel, *et al.*, Reaction of CuO with hydrogen studied by using synchrotron-based x-ray diffraction, *J. Phys.: Condens. Matter*, 2004, **16**(33), S3479.
8 M. S. W. Vong, P. A. Sermon and K. Grant, In-situ study of reduction of copper catalysts, *Catal. Lett.*, 1990, **4**, 15–24.
9 J. Y. Kim, J. A. Rodriguez, J. C. Hanson, *et al.*, Reduction of CuO and Cu_2O with H_2: H embedding and kinetic effects in the formation of suboxides, *J. Am. Chem. Soc.*, 2003, **125**(35), 10684–10692.
10 J. A. Rodriguez, J. Y. Kim, J. C. Hanson, *et al.*, Reduction of CuO in H_2: in situ time-resolved XRD studies, *Catal. Lett.*, 2003, **85**, 247–254.
11 D. Jelić, B. Tomić-Tucaković and S. Mentus, A kinetic study of copper (II) oxide powder reduction with hydrogen, based on thermogravimetry, *Thermochim. Acta*, 2011, **521**(1–2), 211–217.
12 Y. Maimaiti, M. Nolan and S. D. Elliott, Reduction mechanisms of the CuO (111) surface through surface oxygen vacancy formation and hydrogen adsorption, *Phys. Chem. Chem. Phys.*, 2014, **16**(7), 3036–3046.
13 H. Jabraoui, M. D. Rouhani, C. Rossi, *et al.*, First-principles investigation of CuO decomposition and its transformation into Cu_2O, *Phys. Rev. Mater.*, 2022, **6**(9), 096001.
14 B. X. Yang, L. P. Ye, H. J. Gu, *et al.*, A density functional theory study of CO oxidation on CuO_{1-x} (111), *J. Mol. Model.*, 2015, **21**, 1–7.
15 P. Hohenberg and W. Kohn, Inhomogeneous electron gas, *Phys. Rev. [Sect.] B*, 1964, **136**(3), B864.
16 W. Kohn and L. J. Sham, Self-consistent equations including exchange and correlation effects, *Phys. Rev. [Sect.] A*, 1965, **140**(4), A1133.
17 G. Henkelman, B. P. Uberuaga and H. Jónsson, A climbing image nudged elastic band method for finding saddle points and minimum energy paths, *J. Chem. Phys.*, 2000, **113**(22), 9901–9904.
18 G. Henkelman and H. Jónsson, A dimer method for finding saddle points on high dimensional potential surfaces using only first derivatives, *J. Chem. Phys.*, 1999, **111**(15), 7010–7022.
19 G. Kresse and J. Hafner, Ab initio molecular dynamics for liquid metals, *Phys. Rev. B: Condens. Matter Mater. Phys.*, 1993, **47**(1), 558.
20 G. Kresse and J. Furthmüller, Efficiency of ab-initio total energy calculations for metals and semiconductors using a plane-wave basis set, *Comput. Mater. Sci.*, 1996, **6**(1), 15–50.
21 P. E. Blöchl, Projector augmented-wave method, *Phys. Rev. B: Condens. Matter Mater. Phys.*, 1994, **50**(24), 17953.
22 J. P. Perdew, K. Burke and M. Ernzerhof, Generalized gradient approximation made simple, *Phys. Rev. Lett.*, 1996, **77**(18), 3865.
23 H. J. Monkhorst and J. D. Pack, Special points for Brillouin-zone integrations, *Phys. Rev. B: Solid State*, 1976, **13**(12), 5188.
24 L. Wang, T. Maxisch and G. Ceder, Oxidation energies of transition metal oxides within the GGA+ U framework, *Phys. Rev. B: Condens. Matter Mater. Phys.*, 2006, **73**(19), 195107.
25 V. I. Anisimov, J. Zaanen and O. K. Andersen, Band theory and Mott insulators: Hubbard U instead of Stoner I, *Phys. Rev. B: Condens. Matter Mater. Phys.*, 1991, **44**(3), 943.
26 K. Bhola, J. J. Varghese and L. Dapeng, Influence of Hubbard U parameter in simulating adsorption and reactivity on CuO: Combined theoretical and experimental study, *J. Phys. Chem. C*, 2017, **121**(39), 21343–21353.
27 S. Maintz, V. L. Deringer, A. L. Tchougréeff and R. Dronskowski, LOBSTER: A tool to extract chemical bonding from plane-wave based DFT, *J. Comput. Chem.*, 2016, **37**, 1030–1035.
28 K. Momma and F. Izumi, VESTA 3 for three-dimensional visualization of crystal, volumetric and morphology data, *J. Appl. Crystallogr.*, 2011, **44**(6), 1272–1276.
29 A. Hémeryck, A. Motta, C. Lacaze-Dufaure, *et al.*, DFT-D study of adsorption of diaminoethane and propylamine molecules on anatase (101) TiO_2 surface, *Appl. Surf. Sci.*, 2017, **426**, 107–115.
30 S. Åsbrink and L. J. Norrby, A refinement of the crystal structure of copper (II) oxide with a discussion of some exceptional esd's, *Acta Crystallogr., Sect. B: Struct. Crystallogr. Cryst. Chem.*, 1970, **26**(1), 8–15.
31 J. Hu, D. Li, J. G. Lu, *et al.*, Effects on electronic properties of molecule adsorption on CuO surfaces and nanowires, *J. Phys. Chem. C*, 2010, **114**(40), 17120–17126.
32 D. A. Svintsitskiy, T. Y. Kardash, O. A. Stonkus, *et al.*, In situ XRD, XPS, TEM, and TPR study of highly active in CO oxidation CuO nanopowders, *J. Phys. Chem. C*, 2013, **117**(28), 14588–14599.
33 M. García-Melchor and N. López, Homolytic products from heterolytic paths in H_2 dissociation on metal oxides: the example of CeO_2, *J. Phys. Chem. C*, 2014, **118**(20), 10921–10926.
34 J. Reedijk and K. R. Poeppelmeier, *Comprehensive Inorganic Chemistry II: From Elements to Applications*, 2013.
35 V. E. Henrich and P. A. Cox, *The Surface Science of Metal Oxides*, Cambridge University Press, 1994.
36 J. L. G.Fierro, *Metal oxides: chemistry and applications*, CRC press, 2005.

37 X. Yu, C. Zhao, T. Zhang, *et al.*, Molecular and dissociative O_2 adsorption on the Cu_2O (111) surface, *Phys. Chem. Chem. Phys.*, 2018, **20**(31), 20352–20362.
38 T. L. Brown, H. E. LeMay and B. E. Bursten, *Chemistry: The Central Science*, Pearson Educación, 2002.
39 L. Hozoi, L. Siurakshina, P. Fulde, *et al.*, Ab Initio determination of Cu 3d orbital energies in layered copper oxides, *Sci. Rep.*, 2011, **1**(1), 65.
40 Z. Hu, Y. Peng, F. Sun, *et al.*, Thermodynamic equilibrium simulation on the synthesis gas composition in the context of underground coal gasification, *Fuel*, 2021, **293**, 120462.
41 E. R. Monazam, R. W. Breault and R. Siriwardane, Kinetics of magnetite (Fe_3O_4) oxidation to hematite (Fe_2O_3) in air for chemical looping combustion, *Ind. Eng. Chem. Res.*, 2014, **53**(34), 13320–13328.
42 H. A. Alalwan, D. M. Cwiertny and V. H. Grassian, Co_3O_4 nanoparticles as oxygen carriers for chemical looping combustion: a materials characterization approach to understanding oxygen carrier performance, *Chem. Eng. J.*, 2017, **319**, 279–287.
43 T. Mattisson, M. Johansson and A. Lyngfelt, The use of NiO as an oxygen carrier in chemical-looping combustion, *Fuel*, 2006, **85**(5–6), 736–747.